Voltage-Controlled Magnetic Reversal in Orbital Chern Insulators

Jihang Zhu, ¹ Jung-Jung Su, ² and A. H. MacDonald ¹ ¹Department of Physics, University of Texas at Austin, Austin, Texas 78712, USA ²Department of Electrophysics, National Chiao Tung University, Hsinchu 300, Taiwan

(Received 3 March 2020; revised 28 August 2020; accepted 21 October 2020; published 24 November 2020)

Chern insulator ferromagnets are characterized by a quantized anomalous Hall effect and have so far been identified experimentally in magnetically doped topological insulator thin films and in bilayer graphene moiré superlattices. We classify Chern insulator ferromagnets as either spin or orbital, depending on whether the orbital magnetization results from spontaneous spin polarization combined with spin-orbit interactions, as in the magnetically doped topological insulator case, or directly from spontaneous orbital currents, as in the moiré superlattice case. We argue that, in a given magnetic state, characterized, for example, by the sign of the anomalous Hall effect, the magnetization of an orbital Chern insulator will often have opposite signs for weak p and weak p electrostatic or chemical doping. This property enables pure electrical switching of a magnetic state in the presence of a fixed magnetic field.

DOI: 10.1103/PhysRevLett.125.227702

Introduction.—A ferromagnet may be defined as an equilibrium state of matter in which time-reversal (TR) symmetry is broken without lowering translational symmetries. Ferromagnets generically have both nonzero spin magnetization and nonzero orbital magnetization (OM). In almost all ferromagnets, the microscopic mechanism responsible for order is spontaneous spin alignment driven by exchange interactions, which breaks spin-rotational invariance and leads to a nonzero spatially averaged spin moment density. Spin-orbit interactions then play a secondary role by inducing a small parasitic contribution to magnetization from orbital currents and a related nonzero (anomalous) Hall conductivity.

This Letter is motivated by recent experiments [1–6] that have established the quantized anomalous Hall effect (QAHE) in two quite different classes of two-dimensional ferromagnets. The QAHE signals [7,8] the formation of a ferromagnetic state, often referred to as a Chern insulator (CI), with occupied quasiparticle bands whose topological Chern numbers [9] sum to a nonzero value. We find that when ferromagnetism mainly results from spontaneous orbital moments (not spin moments), as in the QAHE states recently discovered [2–4] in magic angle twisted bilayer graphene (MATBG), the magnetizations of weakly n-doped and weakly p-doped insulators can differ in sign in the same magnetic state characterized, for example, by a given sign of the anomalous Hall conductivity. This property could enable magnetic state reversal in the presence of a magnetic field to be achieved purely electrically.

The mechanism that allows the magnetizations of weakly *n*-doped and weakly *p*-doped CIs to differ drastically is closely related to the quantum Hall effect itself. Because of the presence of protected edge states, the OM M

of a CI changes [10] with chemical potential μ even when μ is inside the bulk energy gap:

$$\frac{dM}{du} = \frac{dI}{du} = \frac{Ce}{2\pi\hbar},\tag{1}$$

where C, the Chern index sum, is an integer equal to the Hall conductance in e^2/h units. Equation (1) emphasizes that the quantized Hall conductance can be understood [10] in terms of chiral edge states that are occupied to different chemical potentials along different portions of the sample boundary. It follows from Eq. (1) that the magnetization jumps by $\Delta M = CeE_{\rm gap}/2\pi\hbar$ when the chemical potential jumps across the gap of a CI. Note that the jump in the magnetization depends only on the value of the energy gap and on fundamental constants. We show below that in orbital Chern insulator (OCI) ferromagnets this jump can be sufficient to change the sign of magnetization simply by changing the sign of doping.

Spin Chern insulators.—In magnetically doped topological insulator (MTI) thin films, TR symmetry is broken by introducing local moments that order ferromagnetically. Spin-orbit coupling then leads to an anomalous Hall effect (AHE) that is quantized and to orbital ferromagnetism. To compare the OM jump with the magnitude of the spin magnetization, we express it in units of Bohr magnetons $\mu_B = e\hbar/2m$ per surface unit cell:

$$\frac{\Delta M}{\mu_B/A_{\rm uc}} = \frac{CmA_{\rm uc}E_{\rm gap}}{\pi\hbar^2},\tag{2}$$

where $A_{\rm uc}$ is the area of the surface unit cell. In MTIs, spin magnetization in Bohr magnetons per surface unit cell is typically ~1 because the fraction of sites with magnetic atoms is ~ 0.1 and the number of magnetically doped layers is ~ 10 . Note that the spin magnetization does not depend on the position of the chemical potential within the gap. We see from Eq. (2) that the OM jump across the gap is small compared to the spin magnetization since the surface state energy gap, although not known accurately, is certainly small compared to the $\hbar^2/mA_{\rm uc}$, which depends only on fundamental constants and the surface unit cell area and has a typical value in the 1–10 eV range. For MTIs, and other spin CIs, the unusual jump in the magnetization across the insulator's gap is small in a relative sense and unlikely to have a qualitative influence on magnetic properties.

Orbital Chern insulators.—The Hall conductivity of a CI ferromagnet is quantized when the chemical potential lies in the gap or when carriers introduced by chemical or electrostatic doping are localized. It is convenient to use the sign of the Hall conductivity to distinguish a magnetic state from its TR counterpart. We will refer to the state with positive quantized Hall conductivity Ce^2/h as the + state and to the state with negative quantized Hall conductivity $-Ce^2/h$ as the—state. Although their variations with chemical potential are very distinct, as we emphasize below, both the Hall conductivity $\sigma_H^{\pm}(\mu)$ and OM $M^{\pm}(\mu)$ are orbital fingerprints of broken TR and at any doping level have opposite signs in TR partner states: $M^{-}(\mu) = -M^{+}(\mu)$, $\sigma_H^{-}(\mu) = -\sigma_H^{+}(\mu)$.

The TR symmetry breaking mechanism in the OCIs recently discovered in MATBG devices has been actively discussed in recent work [11–16]. It is almost certainly related to condensation in momentum space, a concept discussed some time ago by Heisenberg and London [17] and previously proposed [18] as a possible symmetry breaking mechanism in metallic gated AB Bernal bilayer graphene. Momentum space condensation is driven by the property that interaction energies in systems with longrange Coulomb interactions can be lowered by occupying states that are more compactly distributed in momentum space than the occupied states of noninteracting bands. Just as exchange interactions in itinerant electron systems occur only between like spins, exchange interactions between states with nearby momenta are stronger than those between states far apart in momentum space. In materials, like graphene, with low energy states located near two widely separated valley centers, momentum space condensation translates to spontaneous valley population polarization. When combined with the intrinsically topological character [19–21] of the valley-projected bands in these materials, valley polarization yields an AHE that is quantized in insulating states. The recently discovered graphene multilayer QAHE states [2–4] provide, as far as we are aware, the only demonstrated example of this mechanism at work. In order to estimate the OM of these states, we apply the convenient envelope function description [22] in which the moiré superlattices are described by a valley-projected periodic Hamiltonian that accounts for position-dependent stacking. We focus below on the case of twisted bilayer graphene (TBG) sandwiched by aligned hexagonal boron nitride (hBN) layers.

OM of TBG on hBN.—The contribution to OM from a single band of 2D Bloch electrons is [9,23–26]

$$M_{n}(\mu) = \int \frac{d^{2}\mathbf{k}}{(2\pi)^{2}} \mathcal{M}_{n}(\mathbf{k}, \mu) f[\mu - \varepsilon_{n}(\mathbf{k})]$$

$$\mathcal{M}_{n}(\mathbf{k}, \mu) = \frac{e}{\hbar} \operatorname{Im} \sum_{n' \neq n} \frac{\langle n | \partial_{x} H | n' \rangle \langle n' | \partial_{y} H | n \rangle}{(\varepsilon_{n} - \varepsilon_{n'})^{2}} (\varepsilon_{n} + \varepsilon_{n'} - 2\mu),$$
(3)

where n is a band index, μ is the chemical potential, $f[\mu - \varepsilon_n(\mathbf{k})]$ is Fermi–Dirac distribution, $\partial_j H = \partial H/\partial k_j$ is the velocity operator, and $|n\rangle$ is a Bloch state with implicit wave-vector dependence. We separate the OM in Eq. (3) into two parts by defining

$$\begin{split} M_{n}^{1}(\mu) &= \frac{e}{\hbar} \text{Im} \sum_{n' \neq n} \int \frac{d^{2}k f_{n}}{(2\pi)^{2}} \frac{\langle n | \partial_{x} H | n' \rangle \langle n' | \partial_{y} H | n \rangle}{(\varepsilon_{n} - \varepsilon_{n'})^{2}} (\varepsilon_{n} + \varepsilon_{n'}) \\ M_{n}^{2}(\mu) &= \frac{e}{\hbar} \text{Im} \sum_{n' \neq n} \int \frac{d^{2}k f_{n}}{(2\pi)^{2}} \frac{\langle n | \partial_{x} H | n' \rangle \langle n' | \partial_{y} H | n \rangle}{(\varepsilon_{n} - \varepsilon_{n'})^{2}} (-2\mu), \end{split}$$

$$(4)$$

where f_n is short for $f[\mu - \varepsilon_n(\mathbf{k})]$. When band n is full, $M_n^1(\mu)$ is independent of μ , whereas $M_n^2(\mu)$ includes the edge state contribution and is proportional to μ with proportionality constant $C_n e/2\pi\hbar$, where C_n is the Chern number of band n.

We now apply these expressions to TBG encapsulated between hBN layers whose influence on the low-energy graphene Hamiltonian is captured [27–33] in part by a mass term representing the spatially averaged difference between carbon π -orbital energies on different honeycomb sublattices. The valley-projected TBG Hamiltonian is $\mathcal{H}(\mathbf{r}) = h_0^{(1)} + h_0^{(2)} + T(\mathbf{r}) + \text{H.c.}$, where $h_0^{(l)}(\mathbf{r}) = -i\partial_x \sigma_x - i\partial_y \sigma_y + m_l \sigma_z$ is the massive Dirac Hamiltonian of layer l, σ acts on the sublattice degrees of freedom, and $T(\mathbf{r})$ is the periodic interlayer tunneling Hamiltonian [22]. The conclusions we reach below rest in part on a particle-hole symmetry property of this Hamiltonian, discussed at greater length in S1 of the Supplemental Material (SM) [34].

$$\tau_z \sigma_x \mathcal{H}(x, y) \sigma_x \tau_z = -\mathcal{H}(-x + d, y) \tag{5}$$

$$\tau_x \mathcal{H}(x, y) \tau_x = \mathcal{H}^*(-x + d, y) \tag{6}$$

In Eqs. (5) and (6), τ acts on the layer degrees of freedom and $d = a_M/\sqrt{3}$ (modulo $\sqrt{3}a_M$) where a_M is moiré lattice constant. Equation (5) states that up to a translation and a change in the sign of the interlayer tunneling term,

sublattice exchange combined with reflection by the *y* axis simply changes the sign of the Hamiltonian. Equation (5) becomes exact in the limit of small twist angles and is accurate in MATBG. Equation (6) is satisfied only when the masses of two graphene layers are identical. In momentum space, the Hamiltonian satisfies

$$\tau_z \sigma_x H(k_x, k_y) \sigma_x \tau_z = -H(-k_x, k_y) \tag{7}$$

$$\tau_x H(k_x, k_y) \tau_x = H^*(k_x, -k_y).$$
 (8)

Given Eq. (7), it can be shown, as detailed in SM S1, that the contribution to OM from a valley vanishes when μ lies in the middle of the gap between the conduction and valence bands of that valley.

For graphene on hBN, m has been estimated using density-functional theory [29-31] to be ~3.6 meV for perfect alignment but can be substantially enhanced by interaction effects absent in density-functional theory and decreases with the relative twist angle. Experimental m values for nearly aligned graphene on hBN are \sim 10–15 meV [45–47]. Figure 1 illustrates the K-valley low-energy moiré bands and Chern numbers of 1.1° TBG for different mass choices. The choice $m_1 = m_2$ [Fig. 1(a)] corresponds to the case in which both graphene layers are aligned and have equivalent stacking orientation relative to their adjacent hBN layers, while $m_1 = -m_2$ [Fig. 1(c)] corresponds to the case in which two graphene layers have opposite relative stacking orientations. $m_1 = 0$ [Fig. 1(b)] corresponds to layer l having a large misalignment relative to hBN so that strain enhancement is absent. We find that gaps (E_q^0) appear at charge neutrality, that the bands are relatively flat for twists near the magic angle, and that they have nonzero Chern numbers when both layers have the same alignment or only one layer is aligned. The case of opposite masses produces trivial bands [Fig. 1(c)]. In all three cases, sublattice symmetry breaking gaps the Dirac

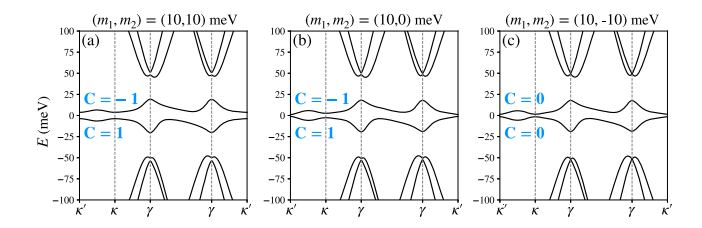


FIG. 1. 1.1°-TBG moiré band structures in valley K for three hBN-induced mass choices. (a) $m_1=m_2=10$ meV produces a band gap $E_g^0 \sim 7.5$ meV at charge neutrality. (b) $m_1=10$, $m_2=0$ meV produces $E_g^0 \sim 2.3$ meV. (c) $m_1=-m_2=-10$ meV produces $E_g^0 \sim 3$ meV. The flat bands are nontrivial with Chern numbers $C=\pm 1$ in (a),(b) and trivial in (c). The moiré bands were calculated using a low-energy continuum model [22] with interlayer tunneling strength $w^{AB}=110$ meV and $w^{AA}/w^{AB}=0.85$ to account for corrugation and strain.

points at the moiré Brillouin zone corners that otherwise link the conduction and valence bands.

SU(4) symmetric mean-field model.—Figure 2(b) plots the single-flavor OM from valleys K and K' (solid lines) at twist angle 1.1° as a function of μ measured relative to the midpoint between its shifted conduction and valence bands. As explained previously, the OM from each valley vanishes at midgap and varies linearly within the gap. Because valleys K and K' are time-reversed counterparts, their magnetization contributions are always opposite in sign.

Because of the fourfold degeneracy of the moiré flat bands [Fig. 2(a)], gaps can appear only at moiré filling factors ν that are multiples of four when interactions are neglected. To account for the CI gaps at odd integer values of ν , we use a simplified but still qualitatively reliable [49] mean-field model in which exchange interactions shift all the band energies of a given flavor en masse—down when the flat conduction band is occupied and up when the flat valence band is emptied [Figs. 2(c)-2(f)]. The band energy shift U must exceed the bandwidth w in order for the gapped state to be self-consistent; this Stoner criterion is easily satisfied near the magic angle because w is extremely small. Schematic ordered state bands for $\nu = 3$ and $\nu = 1$ are plotted in Fig. 2(c) and (e). For three electrons per moiré period ($\nu = 3$), the density at which the QAHE has been most often observed to date, all the majority \downarrow spin's flat bands are occupied and the magnetization contributions from its two valleys cancel. We can therefore consider only the minority ↑ spin bands shown in Fig. 2(d). Similarly, for one electron per moiré period ($\nu = 1$), we can consider only the majority \downarrow spin bands illustrated in Fig. 2(f).

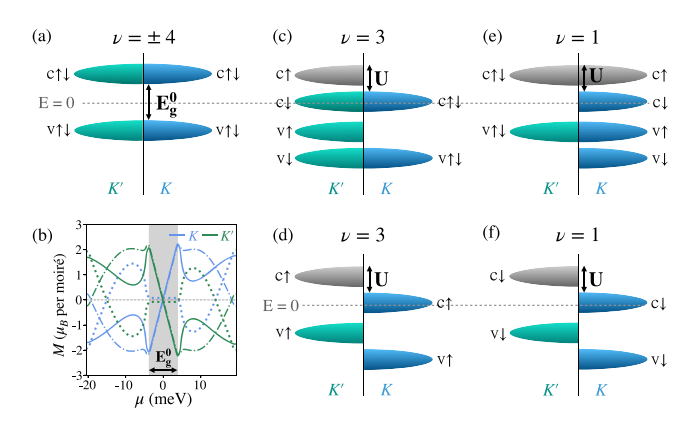


FIG. 2. (a) Schematic moiré flat bands with SU(4) spin and valley flavor symmetry maintained. E_g^0 is the single-particle band gap. "c" and "v" indicate the "conduction" and "valence" bands. (b) OM (solid line) from valleys K (blue) and K' (green) as a function of μ . The dotted and dash-dotted lines are, respectively, the M^1 and M^2 [48] contributions defined in Eq. (4). The single-particle gap is shaded in gray. (c)–(f) Schematic moiré flat bands in TR broken symmetry states at $\nu=3$ and $\nu=1$ in which different flavors are rigidly shifted in energy by a momentum- and flavor-independent exchange energy U if the flat conduction band is filled in that flavor.

Although the magnetization of an OCI can in principle reverse its sign at any filling factor, depending on the details of the Chern band, abrupt reversals vs gate voltage occur only at integer ν , where the magnetization has a large jump. We therefore focus on the magnetization jumps at $\nu=3$ and $\nu=1$; a similar analysis applies for $\nu=-3$ and $\nu=-1$. The total OM is calculated by summing Eq. (3) over spin and valley flavors and bands:

$$M(\mu) = \sum_{m,f} \left(M_{mf}^{1} n_{mf} + \mu \frac{C_{mf} n_{mf}}{2\pi} \right) + U \sum_{m,f \in f_{\text{shift}}} \frac{C_{mf} n_{mf}}{2\pi},$$
(9)

where m is a band index in the valley- and spin-projected continuum model, f is a flavor index, $f_{\rm shift}$ is the set of flavors that have had their energies shifted by -U, n_{mf} is the band occupation, and C_{mf} is the band Chern number. M_{mf}^1 is evaluated with the zero of energy located at the middle of E_g^0 as in Fig. 2(a). The last term in Eq. (9) comes from the magnetization contribution as a result of band energy shift: the OM of an occupied band changes by $-C_{mf}\delta E/2\pi$ when the band energy is rigidly shifted by δE .

Since the magnetizations and Chern numbers of time-reversed bands cancel, i.e., $M_{mK}^1 = -M_{mK'}^1$ and $C_{mK} = -C_{mK'}$, it follows that at both $\nu = 3$ and $\nu = 1$: $\sum_{m,f} (M_{mf}^1 n_{mf} + \mu C_{mf} n_{mf}/2\pi) = M_{cK}^1 + \mu C_{cK}/2\pi.$ The extra magnetization contribution from occupied bands that suffer an exchange energy shift U is $U\sum_{m,f \in f_{\text{shift}}} C_{mf} n_{mf}/2\pi = U(C_{cK} + C_{vK} + C_{v'K})/2\pi$, where $C_{cK}(C_{vK})$ is the Chern number of the flat conduction(valence) band in valley K and $C_{v'K}$ is the total Chern number summed over all remote valence bands.

In our simplified SU(4) symmetric model, M_{cK}^1 and the Chern numbers are purely single-particle properties. For the range of parameters (θ, m) plotted in Fig. 3, $C_{cK} = -C_{vK} = -1$ and $C_{v'K} = 0$. It follows that for both $\nu = 1$ and $\nu = 3$, the magnetization $(M^{\text{n-doped}})$ when μ is at the bottom of unoccupied band(s) is

$$M^{\text{n-doped}} = M \left(\mu = \frac{E_g}{2} \right) = M_{\text{c}K}^1 - \frac{E_g}{4\pi}$$
 (10)

and the magnetization $(M^{\text{p-doped}})$ when μ is at the top of occupied bands is

$$M^{\text{p-doped}} = M\left(\mu = \frac{E_g}{2} - \Delta_g\right) = M_{\text{c}K}^1 - \frac{E_g}{4\pi} + \frac{\Delta_g}{2\pi},$$
 (11)

where $\Delta_g = \min\{U - w, E_g\}$ is the correlated gap at $\nu = 1$, 3. The magnetization sign reverses across the gap if

$$M^{\text{n-doped}} < 0$$
 and $M^{\text{p-doped}} > 0$. (12)

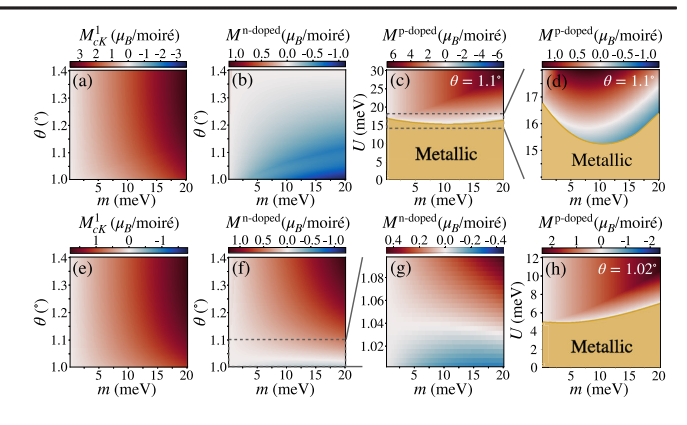


FIG. 3. Plots of M_{cK}^1 , $M^{\text{n-doped}}$, and $M^{\text{p-doped}}$. (a)–(d) With $m_1=m_2=m$. (e)–(g) With $m_1=m$ and $m_2=0$. (a) M_{cK}^1 increases as both θ and m. (b) $M^{\text{n-doped}}(\theta,m)$ is negative in most parts of the parameter range shown in the figure. (c) $M^{\text{p-doped}}(U,m)$ for a typical twist angle $\theta=1.1^\circ$. (d) Enlargement of the dashed rectangle in (c). $M^{\text{p-doped}}$ is positive as long as $\Delta_g \gtrsim 1$ meV. (e) Similar to (a), M_{cK}^1 increases as both θ and m. (f) $M^{\text{n-doped}}(\theta,m)$. (g) Enlargement of the dashed rectangle in (f), $M^{\text{n-doped}}$ is only negative for $\theta \lesssim 1.04^\circ$. (h) Similar to (d), $M^{\text{p-doped}}$ is positive for a tiny gap. In (c),(d),(h), the parameter region where U < w is identified to be metallic.

In Fig. 3(a), we show that M_{cK}^1 increases as a function of both θ and mass $m=m_1=m_2$. Figure 3(b), which plots $M^{\text{n-doped}}(\theta,m)$, reveals that the first condition in Eq. (12) is always satisfied near the magic twist angle. Figure 3(c) plots $M^{\text{p-doped}}(U,m)$ for a typical twist angle $\theta=1.1^\circ$. Insulating states occur only when U>w. We find that $M^{\text{p-doped}}$ is almost always positive, satisfying the second condition in Eq. (12), although there is a small no-reversal region in which the CI gap $\Delta_g=U-w\sim 1$ meV that is highlighted in Fig. 3(d). Similar results for $m_1=m,m_2=0$ models are provided in Figs. 3(e)–3(h). In this case, $M^{\text{n-doped}}$ is negative for $\theta\lesssim 1.04^\circ$, as illustrated in Fig. 3(g).

Discussion.—CIs are 2D electron systems with charge gaps that exhibit QAHE and have now been realized experimentally by two distinct mechanisms. In MTI [1,50–55], the QAHE is driven by the exchange interactions between spin local moments that order ferromagnetically and two Dirac-cones localized on opposite surfaces of a topological insulator thin film. In TBG, on the other hand, the QAHE is driven by broken sublattice symmetry, which gaps Dirac cones and induces Berry curvatures of opposite signs near TR-partner valleys, combined with TR symmetry breaking via condensation of electrons into one of the two valleys. Both experimentally established QAHE mechanisms differ from the one identified in the original theoretical work of Haldane [8] in which the QAHE is driven by broken TR symmetry that leads to Berry curvatures of the same sign near opposite valleys.

In TBG, sublattice polarization is theoretically expected to occur spontaneously but can be enforced by alignment with hBN. Spontaneous valley polarization and spin polarization are then energetically preferred when the moiré bands are narrowed by tuning the orientation close to the magic angle. Because of the absence of substantial spinorbit coupling in graphene, the orbital valley order has an Ising character and is therefore essential to achieve a finite transition temperature. It is also dominantly responsible for the magnetization and solely responsible for the most accessible observable: the OAHE. We have shown in this Letter that the dominance of OM changes the considerations [56] that normally limit our ability to control magnetic states electrically. The most extreme example of the strong electrical effects that are possible in OCIs is a consequence of the jump in magnetization between weak ndoping and weak p doping produced by edge states. Changing the sign of magnetization of a state with a given sign of valley polarization and QAHE changes the thermodynamically preferred state in a weak magnetic field purely electrically. This property could be of technological value if other examples of OCIs that have higher transition temperatures are discovered in the future. When the sign of the magnetization is independent of carrier density, the Středa [57] formula implies that magnetic switching between QAHE states will yield stronger transport signals for either n or p doping, depending on the relative sign of magnetization and Hall conductivity. This behavior is common in current experiments [3,4,21,58,59]. As illustrated in SM S3, QAHE sign switching that is equally robust for n and pdopings signals the magnetization reversal that we expect to be common in large gap OCIs.

In our simplified mean-field theory, the magnetizations at weak n and p dopings are identical at $\nu=3$ and $\nu=1$ since Eqs. (9)–(11) apply to both cases. This property is a consequence not only of the simplified mean-field theory but also of our neglect of correlations, which are likely to play an important role in determining whether or not CI states appear. Since the flat-band system has more phase space for correlations closer to charge neutrality, we anticipate that CI states will be more common at $\nu=\pm3$, than at $\nu=\pm1$.

J. Z. was supported by the National Science Foundation through the Center for Dynamics and Control of Materials: an NSF MRSEC under Cooperative Agreement No. DMR-1720595. A. H. M. was supported by DOE BES Grant No. FG02-02ER45958. The authors acknowledge resources provided by the Texas Advanced Computing Center (TACC) at The University of Texas at Austin that have contributed to the research results reported in this Letter.

Note added.—While this manuscript was under review, the magnetization sign reversal it predicts was observed in twisted monolayer on bilayer graphene and in TBG [60].

- X. Chen, J. Jia, X. Dai, Z. Fang, S.-C. Zhang, K. He, Y. Wang, L. Lu, X.-C. Ma, and Q.-K Xue, Science **340**, 167 (2013).
- [2] A. L. Sharpe, E. J. Fox, A. W. Barnard, J. Finney, K. Watanabe, T. Taniguchi, M. A. Kastner, and D. Goldhaber-Gordon, Science 365, 605 (2019).
- [3] G. Chen, A. L. Sharpe, E. J. Fox, Y.-H. Zhang, S. Wang, L. Jiang, B. Lyu, H. Li, K. Watanabe, T. Taniguchi, Z. Shi, T. Senthil, D. Goldhaber-Gordon, Y. Zhang, and F. Wang, Nature (London) 579, 56 (2020).
- [4] M. Serlin, C. L. Tschirhart, H. Polshyn, Y. Zhang, J. Zhu, K. Watanabe, T. Taniguchi, L. Balents, and A. F. Young, Science 367, 900 (2019).
- [5] H. Polshyn, J. Zhu, M. A. Kumar, Y. Zhang, F. Yang, C. L. Tschirhart, M. Serlin, K. Watanabe, T. Taniguchi, A. H. MacDonald, and A. F. Young, arXiv:2004.11353.
- [6] S. Chen, M. He, Y.-H. Zhang, V. Hsieh, Z. Fei, K. Watanabe, T. Taniguchi, D. H. Cobden, X. Xu, C. R. Dean, and M. Yankowitz, arXiv:2004.11340.
- [7] D. J. Thouless, M. Kohmoto, M. P. Nightingale, and M. den Nijs, Phys. Rev. Lett. 49, 405 (1982).
- [8] F. D. M. Haldane, Phys. Rev. Lett. 61, 2015 (1988).
- [9] D. Xiao, M.-C. Chang, and Q. Niu, Rev. Mod. Phys. 82, 1959 (2010).
- [10] A. H. MacDonald, arXiv:cond-mat/9410047.
- [11] N. Bultinck, S. Chatterjee, and M. P. Zaletel, Phys. Rev. Lett. **124**, 166601 (2020).
- [12] C. Repellin, Z. Dong, Y.-H. Zhang, and T. Senthil, Phys. Rev. Lett. 124, 187601 (2020).
- [13] Y.-H. Zhang, D. Mao, and T. Senthil, Phys. Rev. Research 1, 033126 (2019).
- [14] F. Wu and S. Das Sarma, Phys. Rev. Lett. 124, 046403 (2020).
- [15] Y. Alavirad and J. D. Sau, arXiv:1907.13633 [Phys. Rev. B (to be published)].
- [16] J. Liu and X. Dai, arXiv:1911.03760.
- [17] F. London, Phys. Rev. 74, 562 (1948).
- [18] J. Jung, M. Polini, and A. H. MacDonald, Phys. Rev. B 91, 155423 (2015).
- [19] H. C. Po, L. Zou, T. Senthil, and A. Vishwanath, Phys. Rev. B 99, 195455 (2019).
- [20] Z. Song, Z. Wang, W. Shi, G. Li, C. Fang, and B. A. Bernevig, Phys. Rev. Lett. 123, 036401 (2019).
- [21] X. Lu, P. Stepanov, W. Yang, M. Xie, M. A. Aamir, I. Das, C. Urgell, K. Watanabe, T. Taniguchi, G. Zhang, A. Bachtold, A. H. MacDonald, and D. K. Efetov, Nature (London) 574, 653 (2019).
- [22] R. Bistritzer and A. H. MacDonald, Proc. Natl. Acad. Sci. U.S.A. 108, 12233 (2011).
- [23] T. Thonhauser, D. Ceresoli, D. Vanderbilt, and R. Resta, Phys. Rev. Lett. 95, 137205 (2005).
- [24] D. Ceresoli, T. Thonhauser, D. Vanderbilt, and R. Resta, Phys. Rev. B 74, 024408 (2006).
- [25] R. Bianco and R. Resta, Phys. Rev. Lett. 110, 087202 (2013).
- [26] R. Bianco and R. Resta, Phys. Rev. B 93, 174417 (2016).
- [27] J. R. Wallbank, A. A. Patel, M. Mucha-Kruczyński, A. K. Geim, and V. I. Fal'ko, Phys. Rev. B 87, 245408 (2013).
- [28] P. Moon and M. Koshino, Phys. Rev. B 90, 155406 (2014).
- [29] J. Jung, A. M. DaSilva, A. H. MacDonald, and S. Adam, Nat. Commun. 6, 6308 (2015).

^[1] C.-Z. Chang, J. Zhang, X. Feng, J. Shen, Z. Zhang, M. Guo, K. Li, Y. Ou, P. Wei, L.-L. Wang, Z.-Q. Ji, Y. Feng, S. Ji,

- [30] J. Jung, E. Laksono, A. M. DaSilva, A. H. MacDonald, M. Mucha-Kruczyński, and S. Adam, Phys. Rev. B 96, 085442 (2017).
- [31] J. Jung, A. Raoux, Z. Qiao, and A. H. MacDonald, Phys. Rev. B 89, 205414 (2014).
- [32] M. Kindermann, B. Uchoa, and D. L. Miller, Phys. Rev. B 86, 115415 (2012).
- [33] J. Shi, J. Zhu, and A. H. MacDonald (to be published).
- [34] See Supplemental Material, which includes Refs. [14, 35–44], at http://link.aps.org/supplemental/10.1103/PhysRevLett.125.227702 for the estimation of the spin magnetization in TBG.
- [35] Y. H. Kwan, Y. Hu, S. H. Simon, and S. A. Parameswaran, arXiv:2003.11560.
- [36] A. Kumar, M. Xie, and A. H. MacDonald (to be published).
- [37] T. Holstein and H. Primakoff, Phys. Rev. 58, 1098 (1940).
- [38] N. D. Mermin and H. Wagner, Phys. Rev. Lett. 17, 1133 (1966).
- [39] C. L. Kane and E. J. Mele, Phys. Rev. Lett. 95, 226801 (2005).
- [40] H. Min, J. E. Hill, N. A. Sinitsyn, B. R. Sahu, L. Kleinman, and A. H. MacDonald, Phys. Rev. B 74, 165310 (2006).
- [41] Y. Yao, F. Ye, X. L. Qi, S. C. Zhang, and Z. Fang, Phys. Rev. B **75**, 041401(R) (2007).
- [42] S. Konschuh, M. Gmitra, and J. Fabian, Phys. Rev. B 82, 245412 (2010).
- [43] J. C. Boettger and S. B. Trickey, Phys. Rev. B 75, 121402 (R) (2007).
- [44] P. Streda, J. Phys. C 15, L1299 (1982).
- [45] R.-P. Rebeca, C. Zhang, K. Watanabe, T. Taniguchi, J. Hone, and C. R. Dean, Science 361, 690 (2018).
- [46] N. R. Finney, M. Yankowitz, L. Muraleetharan, K. Watanabe, T. Taniguchi, C. R. Dean, and J. Hone, Nat. Nanotechnol. 14, 1029 (2019).
- [47] B. Hunt, J. D. Sanchez-Yamagishi, A. F. Young, M. Yankowitz, B. J. LeRoy, K. Watanabe, T. Taniguchi, P. Moon, M. Koshino, P. Jarillo-Herrero, and R. C. Ashoori, Science 340, 1427 (2013).
- [48] Note that M^2 (dash-dotted line) should vanish when the flat bands are completely filled or completely empty because the

- total Chern number of all occupied bands is zero in both cases. The numerical error in Fig. 2(b) is difficult to eliminate completely because small inaccuracies in the Berry curvature integrals are magnified when multiplied by a finite chemical potential μ .
- [49] M. Xie and A. H. MacDonald, Phys. Rev. Lett. 124, 097601 (2020).
- [50] J. G. Checkelsky, R. Yoshimi, A. Tsukazaki, K. S. Takahashi, Y. Kozuka, J. Falson, M. Kawasaki, and Y. Tokura, Nat. Phys. 10, 731 (2014).
- [51] X. Kou, S.-T. Guo, Y. Fan, L. Pan, M. Lang, Y. Jiang, Q. Shao, T. Nie, K. Murata, J. Tang, Y. Wang, L. He, T.-K. Lee, W.-L. Lee, and K. L. Wang, Phys. Rev. Lett. 113, 137201 (2014).
- [52] A. J. Bestwick, E. J. Fox, X. Kou, L. Pan, K. L. Wang, and D. Goldhaber-Gordon, Phys. Rev. Lett. 114, 187201 (2015).
- [53] C.-Z. Chang, W. Zhao, D. Y. Kim, H. Zhang, B. A. Assaf, D. Heiman, S.-C. Zhang, C. Liu, M. H. W. Chan, and J. S. Moodera, Nat. Mater. 14, 473 (2015).
- [54] M. Mogi, R. Yoshimi, A. Tsukazaki, K. Yasuda, Y. Kozuka, K. S. Takahashi, M. Kawasaki, and Y. Tokura, Appl. Phys. Lett. 107, 182401 (2015).
- [55] J. Jiang, D. Xiao, F. Wang, J.-H. Shin, D. Andreoli, J. Zhang, R. Xiao, Y.-F. Zhao, M. Kayyalha, L. Zhang, K. Wang, J. Zang, C. Liu, N. Samarth, M. H. W. Chan, and C.-Z. Chang, arXiv:1901.07611.
- [56] B. Dieny and M. Chshiev, Rev. Mod. Phys. 89, 025008 (2017).
- [57] P. Streda, J. Phys. C 15, L717 (1982).
- [58] L. Wang, E.-M. Shih, A. Ghiotto, L. Xian, D. A. Rhodes, C. Tan, M. Claassen, D. M. Kennes, Y. Bai, B. Kim, K. Watanabe, T. Taniguchi, X. Zhu, J. Hone, A. Rubio, A. Pasupathy, and C. R. Dean, Nat. Mater. 19, 861 (2020).
- [59] P. Stepanov, I. Das, X. Lu, A. Fahimniya, K. Watanabe, T. Taniguchi, F. H. L. Koppens, J. Lischner, L. Levitov, and D. K. Efetov, arXiv:1911.09198.
- [60] H. Polshyn, J. Zhu, M. A. Kumar, Y. Zhang, F. Yang, C. L. Tschirhart, M. Serlin, K. Watanabe, T. Taniguchi, A. H. MacDonald, and A. F. Young, arXiv:2004.11353.